

The origin of the UV/optical lags in NGC 5548

Emma Gardner[★] and Chris Done

Centre for Extragalactic Astronomy, Department of Physics, University of Durham, South Road, Durham DH1 3LE, UK

Accepted 2017 April 14. Received 2017 April 14; in original form 2016 March 31

ABSTRACT

The new multiwavelength monitoring campaign on NGC 5548 shows clearly that the variability of the ultraviolet (UV)/optical light curves lags by progressively longer times at longer wavelengths, as expected from reprocessing off an optically thick disc, but that the time-scales are longer than expected for a standard Shakura–Sunyaev accretion disc. We build a full spectral-timing reprocessing model to simulate the UV/optical light curves of NGC 5548. We show that disc reprocessing of the observed hard X-ray light curve produces optical light curves with too much fast variability as well as too short a lag time. Suppressing the fast variability requires an intervening structure preventing the hard X-rays from illuminating the disc. We propose this is the disc itself, perhaps due to atomic processes in the UV lifting the photosphere, increasing the scaleheight, making it less dense and less able to thermalize, so that it radiates low-temperature Comptonized emission as required to produce the soft X-ray excess. The outer edge of the puffed-up Comptonized disc region emits far-UV (FUV) flux, and can illuminate the outer thin blackbody disc, but while this gives reprocessed variable emission that is much closer to the observed UV and optical light curves, the light travel lags are still too short to match the data. We reverse engineer a solution to match the observations and find that the luminosity and temperature of the lagged emission are not consistent with material at the light travel lag distance responding to the irradiating flux (either FUV or X-ray). We conclude that the UV/optical lags of NGC 5548 are neither the light travel time from X-ray reprocessing nor the light travel time from FUV reprocessing, but instead could be the time-scale for the outer blackbody disc vertical structure to respond to the changing FUV illumination.

Key words: accretion, accretion discs – black hole physics – galaxies: active – galaxies: individual: NGC 5548 – galaxies: Seyfert – X-rays: galaxies.

1 INTRODUCTION

The emission from active galactic nuclei (AGN) is typically variable, with faster variability seen at shorter wavelengths. This variability can be used as a tool to probe the surrounding structures, with reverberation mapping of the broad-line region (BLR) being an established technique. However, the same techniques can be used to probe the structure of the accretion flow itself. Hard X-ray illumination of the disc should produce a lagged and smeared thermal reprocessing signal. Larger radii in the disc produce lower temperature emission, so this disc reprocessing picture predicts longer lags at longer wavelengths. Such differential lags are now starting to be seen (Sergeev et al. 2005; McHardy et al. 2014; Edelson et al. 2015; Fausnaugh et al. 2016; McHardy et al. 2016), confirming qualitatively that we are indeed seeing reprocessing from radially extended, optically thick material, as expected from a disc.

However, quantitatively, the picture runs into difficulties. It has long been known that the implied size scales are larger by a factor of a few compared to the expected sizes from a Shakura–Sunyaev disc (e.g. Cackett, Horne & Winkler 2007). Independent size-scale estimates from microlensing also imply that the optical/ultraviolet (UV) emission region is larger than expected by a similar factor (e.g. Morgan et al. 2010). Yet, the optical/UV spectrum shows a strong rise to the blue, and can be fairly well fitted by the emission expected from the outer disc regions in a Shakura–Sunyaev model (e.g. Jin, Ward & Done 2012; Capellupo et al. 2015), though there are discrepancies in detail (e.g. Davis, Woo & Blaes 2007).

Thus, qualitatively, the disc reprocessing picture appears sound, yet, quantitatively, it fails to match the data. This is perhaps not surprising for several reasons. Irradiation can change the structure of the disc, for example, by flaring it, as well as by changing the local heating (Cunningham 1976). Secondly, the spectra of AGN are clearly not simply a disc. The hard X-ray corona itself must be powered by accretion, pointing to a change from a pure Shakura–Sunyaev disc structure in the inner regions (e.g. Done et al. 2012).

* E-mail: e.l.gardner@dur.ac.uk

There is also the generic additional component seen in AGN, the soft X-ray excess, which again points to some change in disc structure that is not captured by the simple Shakura–Sunyaev equations (e.g. Gierliński & Done 2004; Porquet et al. 2004).

Here, we use the unprecedented *Swift* and *Hubble Space Telescope (HST)* light curves collected by the 2014 campaign on NGC 5548, which span 120 d with sampling of 0.5 d, across nine continuum bands from *V* to hard X-rays (Edelson et al. 2015). On long (month–year) time-scales, the optical and X-ray light curves are well correlated, but the optical light curves show more variability than the hard X-rays, ruling out the simplest reprocessing models as accounting for all the optical variability in this source (Uttley et al. 2003; see also Arévalo et al. 2008, 2009). However, on day time-scales, the optical light curves lag behind the X-rays, with lag times increasing with wavelength, as expected from disc reprocessing, and this is sampled in unprecedented detail by the 2014 campaign light curves. We use these to quantitatively test disc reprocessing models using a full model of illumination and reprocessing, with the aim to reproduce both the spectrum and variability of the source.

We first examine traditional disc reprocessing models and confirm that these cannot explain the lag time-scales of the optical/UV light curves of NGC 5548. However, these quantitative models reveal another more fundamental conflict, which is that the UV and optical light curves cannot be produced by reprocessing of the observed hard X-ray flux. Disc reprocessing smears the variability by a similar time-scale to the lag. The UV and optical are lagged by 1–2 d, but are much smoother than the hard X-ray light curve, with no sign of the rapid 1–2 d variability seen in the X-rays (see also Arévalo et al. 2008, and the discussion of variability in Lawrence 2012). This clearly shows that the fast hard X-ray variability is not seen by the outer disc, so not only are the observed X-rays not the driver for reprocessing, but the outer disc must be shielded from the observed X-rays. Instead, the far-ultraviolet (FUV, represented by the *HST* light curve) is a much better match to the observed smoothness of the optical/UV light curves of NGC 5548. We incorporate these two aspects together in a model where the soft X-ray excess is produced from the inner regions of a moderately thickened disc that emits optically thick Compton (hence, we name it the Comptonized disc) and shields the outer blackbody (BB) disc from direct hard X-ray illumination from the central corona. The observed difference between the FUV and soft X-ray light curves clearly shows that this is not a single component, so we assume that the outer regions of the thickened Comptonized disc structure produce the FUV, which can illuminate the outer thin BB disc. However, this still predicts light travel time lags that are shorter than observed. Increased flaring of the outer BB disc does not help because these large radii regions with the required long lag times are too cool to contribute significant optical flux due to their large area.

We explore the suggestion that the longer than expected lags come from the contribution of the classic BLR ($H\beta$ line) to the optical and UV emission (Korista & Goad 2001), but this does not work either as these do not contribute enough lagged flux. Since all known models fail, we reverse engineer a geometry that can fit both spectral and variability constraints. We use the observed optical lags in the different wavelength bands to constrain the luminosity and temperature of BB components at different lag times. We find that the observations can be well matched by a single BB component lagged by 6 d behind the FUV irradiation, consistent with reprocessing on a population of clouds interior to the classic BLR, as suggested by Lawrence (2012). However, the derived area of the reprocessor at this light travel time distance is far too small to intercept enough of the AGN luminosity (either FUV, X-ray or

total) to give the observed luminosity of the lagged component. We conclude that the reprocessing time-scale is not set by the light travel time. Interestingly, the temperature of the required lagged component is close to 10^4 K, which is the trigger for the onset of the dramatic disc instability connected to hydrogen ionization (see e.g. Lasota 2001), so it could instead be linked to the changing structure of the disc at this point.

Fundamentally, the time lags give us the wrong answers because the reverberation signal is not from a thin BB disc responding on the light travel time to illumination by either X-rays or FUV. We suggest that it is instead from the inner edge of the thin BB disc changing its structure in response to an increase in FUV illumination and expanding on the vertical time-scale to join the larger scaleheight Comptonized disc region.

2 energetics of disc illumination and reprocessing

For all models, we fix $M = 3.2 \times 10^7 M_{\odot}$ (as used by Edelson et al. 2015, from Pancoast et al. 2014 : see also their erratum Pancoast et al. 2015). This is similar to the Denney et al. (2010) estimate of $4.4 \times 10^7 M_{\odot}$, though a factor of ~ 2 smaller than the Bentz et al. (2010) estimate of $7.8^{+1.9}_{-2.7} \times 10^7 M_{\odot}$. We also fix distance $D = 75$ Mpc and spin $a = 0$, and assume an inclination angle of 45° .

The unabsorbed, dereddened broad-band spectrum of NGC 5548 from 2013 Summer is shown in Mehdipour et al. (2015). The X-ray flux is very hard, with photon index $\Gamma = 1.6$, and the X-rays dominate the energy output of the source, peaking in νF_{ν} at $\sim 8 \times 10^{-11}$ erg cm^{-2} s^{-1} at 100 keV. The simultaneous optical/UV spectrum looks similar to that expected from an outer thin BB disc (though its shape is subtly different; Mehdipour et al. 2015). The flux in *UVWI* (at around 5 eV) has $\nu F_{\nu} \approx 5 \times 10^{-11}$ erg cm^{-2} s^{-1} .

We use the `OPTXAGNF` model in `XSPEC` to find reasonable physical parameters for the accretion flow. This assumes that the mass accretion rate is constant with radius, with fully relativistic Novikov–Thorne emissivity per unit area, $L_{\text{NT}}(r)$, with dimensionless radius $r = R/R_g$ for $R_g = GM/c^2$, but also assumes that this energy is dissipated in a (colour–temperature–corrected) BB disc down to only some radius r_{cor} , with the remainder split between powering an optically thick Compton component (which provides the soft X-ray excess emission) and an optically thin Compton component, which models the hard X-ray coronal emission. This code calculates the angle-averaged spectrum, so we boost the normalization by a factor of $\cos i / \cos 60 = 1.41$ to roughly account for our assumed inclination angle. If we assume that all the power within $r_{\text{cor}} = 70$ goes to make the hard X-ray corona ($f_{\text{cor}} = 1$), we find that we can match the *UVWI* and X-ray flux for $\log L/L_{\text{Edd}} = -1.4$ with $r_{\text{cor}} = 70$.

This does not necessarily mean that the geometrically thin BB disc itself is not present below $70 R_g$, but only that the accretion power is not dissipated within this structure (Svensson & Zdziarski 1994; Petrucci et al. 2010). However, there is additional information in the hard X-ray spectrum that does point to this conclusion. An optically thick BB disc cannot be present underneath an isotropically emitting corona in this object, as such a disc will intercept around half of the hard X-ray flux, giving a strong Compton hump that is not present in the NuSTAR data (see the spectrum in Mehdipour et al. 2015 and Ursini et al. 2015). Thermalization of the non-reflected emission also produces too many seed photons for the X-ray source to remain hard (Haardt & Maraschi 1991, 1993; Stern et al. 1995; Malzac, Dumont & Mouchet 2005; Petrucci et al. 2013). Together,

these imply that either the X-ray source is very anisotropic or the disc truly truncates for sources with hard X-ray spectra.

Black hole binaries similarly show hard X-ray spectra and small Compton humps in their low/hard state, but here there are clear limits on the possible anisotropy from comparing sources with different binary inclination angles (Heil, Uttley & Klein-Wolt 2015). This argues strongly for true truncation of the BB accretion disc, as does the currently popular Lense–Thirring precession model for the origin of the low-frequency QPOs seen in high-inclination binary systems (Ingram, Done & Fragile 2009). Hence, we assume that the BB disc is truly truncated in these low-luminosity AGN (see also Petrucci et al. 2013; Noda 2016).

The irradiation pattern strongly depends on the relative geometry of the hard X-ray source and BB disc. In the black hole binaries, there is evidence from the complex pattern of energy-dependent lags that the hard X-ray source is somewhat radially extended (Kotov, Churazov & Gilfanov 2001; Ingram & Done 2012), as is also expected if it is some form of hot, radiatively inefficient accretion flow such as an advection-dominated accretion flow (Narayan & Yi 1995). We assume that the extended hard X-ray source has volume emissivity $\propto L_{\text{NT}}(r)/r$ and we neglect light bending and red/blueshifts to work out the irradiating flux, as in the appendix of Zycki, Done & Smith (1999), i.e.

$$F_{\text{rep}}(r) = \frac{f_{\text{irr}} L_{\text{cor}} \cos(n)}{4\pi(\ell R_g)^2}, \quad (1)$$

where ℓ is the distance from the hard X-ray source to the disc surface element, n is the angle between the source and normal to the disc and f_{irr} is the fraction of coronal hard X-ray luminosity (L_{cor}) that thermalizes. We set $f_{\text{irr}} = 1$ in this section in order to see the maximum irradiation flux. We then assume that

$$T_{\text{eff}}(r) = T_{\text{grav}}(r) \left(\frac{F_{\text{rep}}(r) + F_{\text{grav}}(r)}{F_{\text{grav}}(r)} \right)^{1/4}, \quad (2)$$

and model the resulting optically thick disc emission at this radius as a (colour–temperature–corrected) BB. However, the colour–temperature correction makes very little difference for the black hole mass, mass accretion rate and r_{cor} used here, as the disc peaks at 5.5 eV ($\sim 2500 \text{ \AA}$) so is too cool for the colour–temperature correction to be significant.

We first assume that the extended X-ray source illuminates a flat BB disc (formally, we give this disc a constant height of $h = H/R_g = 0.1$). The green dashed line in Fig. 1 shows the resulting irradiation flux per unit area on the equatorial plane. This is $\propto r^{-3}$ at large r , similar to the intrinsic gravitational flux dissipation (red), and is around 10–20 per cent of the intrinsic flux at each radius. We compare this to the mathematically simpler form of a lamppost at height $h_x = 10$ (cyan dotted line, where $h_x = H_x/R_g$) illuminating the BB disc, and show that the two are comparable at all disc radii. This is important as it shows that using lamppost illumination is not necessarily the same as assuming that the source is a lamppost (compact source on the spin axis). The more physical extended source geometry is identical in its illumination properties to the mathematically simpler lamppost.

It is unlikely that the BB disc remains flat under illumination. Cunningham (1976) shows that the disc structure responds to illumination, and can form a flared disc with height $h = h_0(r/r_0)^{9/7}$, where h_0 is the disc height at its outer radius r_0 . We show the resulting illumination for an extended X-ray source (Fig. 1, magenta dashed line), and a lamppost source of height $h_x = 10$ (blue dotted line) and a central source ($h_x = 0$, black dotted line) for a flared disc with $h/r = 0.1$ at $r = 660$. Clearly irradiation can dominate over

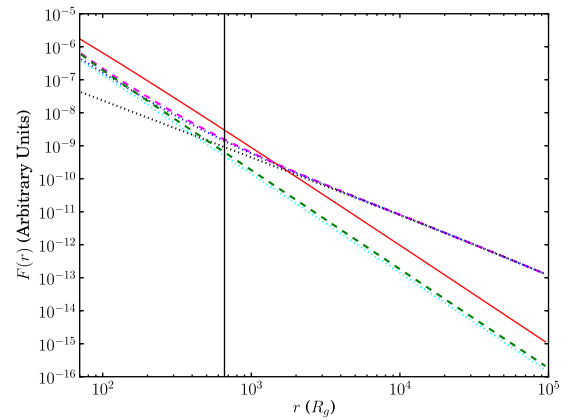


Figure 1. Illuminating flux as a function of BB disc radius. Green and magenta dashed lines show flat ($h = 0.1$) and flared ($h = h_0(r/r_0)^{9/7}$, where $h/r = 0.1$ at $r = 660$) discs, respectively, irradiated by an extended spherical source with $r = 70$. The cyan and blue dotted lines show the same flat and flared discs, respectively, illuminated by a central point source with height $h_x = 10$. The black dotted line shows the flared disc illuminated by a central point source with $h_x = 0$. The red solid line shows the gravitational flux dissipation of the BB disc. The black solid line shows the self-gravity radius.

gravitational energy release for such a flared disc, but only at large radii.

Crucially, irradiation changes the predicted lag-wavelength profile of the BB disc. The standard argument for a lag time $\tau \propto \lambda^{4/3}$ comes from assuming that the wavelength at which the disc peaks at each radius is $\lambda_{\text{max}} \propto 1/T \propto L_{\text{NT}}(r)^{-1/4} \propto (M\dot{M})^{-1/4} R^{3/4}$. Hence, $R \propto \tau \propto (M\dot{M})^{1/3} \lambda_{\text{max}}^{4/3}$. However, in the irradiation-dominated region, the emissivity $L(r) \propto r^{-12/7}$, so the lags are no longer expected to go as $\tau \propto \lambda^{4/3}$ but as $\propto \lambda^{7/3}$.

Fig. 1 shows that irradiation only gives $L(r)$ that is substantially different from r^{-3} at $r > 2000$, so all our irradiation models predict $\tau \propto \lambda_{\text{max}}^{4/3}$ for $r < 1000$. The self-gravity radius for a disc with these parameters is only $660 R_g$ (black vertical line; Laor & Netzer 1989, using Shakura–Sunyaev $\alpha = 0.1$), so that truncating the BB disc at this point means that irradiation never dominates, and there is only a factor of ~ 2 difference between the flared and flat disc illumination fluxes at $r = 660$.

In the following reprocessing models, we wish to maximize irradiation. We therefore use the lamppost at $h_x = 10$ illuminating a flared BB disc (Fig. 1, blue dotted line; illumination pattern identical to an extended spherical source with $r = 70$) in all subsequent models.

2.1 Calculation of cross-correlation functions

Throughout this paper, we compare lags between light curves by calculating the cross-correlation function (CCF). For two light curves $x(t)$ and $y(t)$, which are evenly sampled on time Δt so $t = t_0 + i\Delta t$, the CCF as a function of lag time $\tau = j\Delta t$ is defined as

$$\text{CCF}(\tau) = \frac{\sum (x(i) - \bar{x})(y(i-j) - \bar{y})}{[(\sigma_x^2 - \sigma_{ex}^2)(\sigma_y^2 - \sigma_{ey}^2)]^{1/2}}, \quad (3)$$

where the sum is over all data that contribute to the lag measurement, so there are a smaller number of points for longer lags. The averages, (\bar{x}, \bar{y}) , and measured variances, (σ_x^2, σ_y^2) , and error bar variances $(\sigma_{ex}^2, \sigma_{ey}^2)$, are also recalculated for each τ over the range of data

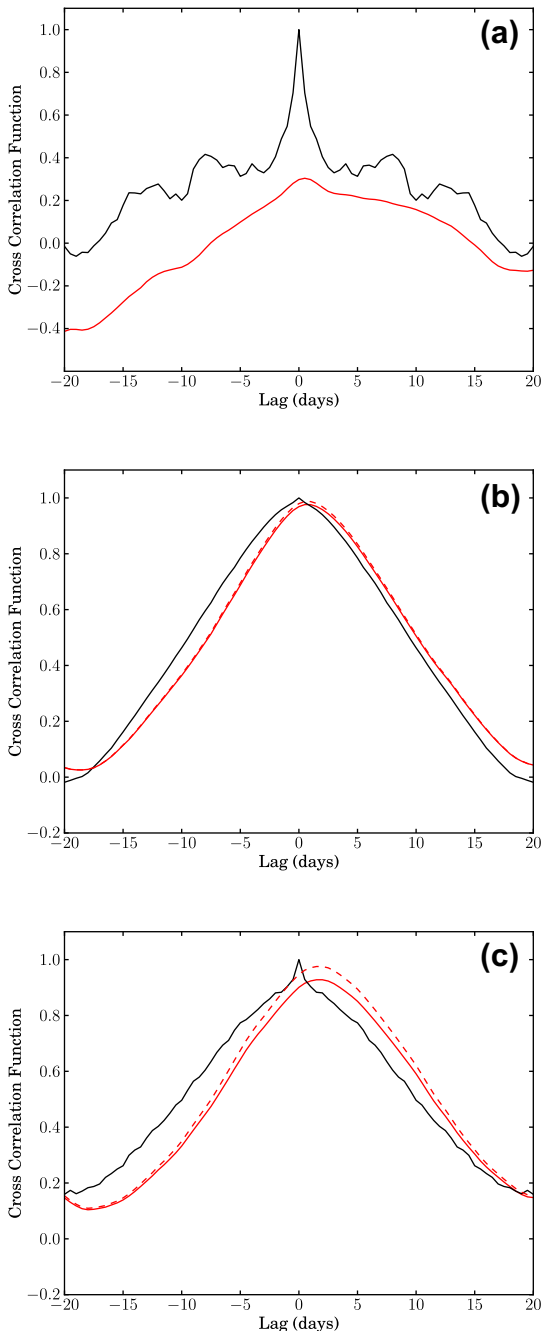


Figure 2. Solid red lines show CCFs calculated from the observed light curves of NGC 5548: (a) FUV with respect to hard X-rays; (b) UVW1 with respect to FUV; and (c) V band with respect to FUV. Solid black lines in (a)–(c) show the ACFs of the hard X-ray, UVW1 and V bands, respectively. The narrow peaks at zero lag in (b) and (c) are due to correlated errors introduced by interpolating the light curves. Red dashed lines in (b) and (c) show the CCFs (UVW1 with respect to FUV and V band with respect to FUV, respectively) after correcting for these correlated errors.

used. With this definition, $\text{CCF}(\tau) = 1$ then implies a complete correlation.

However, real data are not exactly evenly sampled. Interpolation is often used to correct for this, but this can be done in multiple ways (Gaskell & Peterson 1987). The red solid lines in Fig. 2 show the interpolated CCF, computed by linearly interpolating both light

curves on to a grid of 0.1 d spacing and then resampling to produce evenly sampled light curves with $dt = 0.5$ d. This interpolation scheme introduces correlated errors, and it is not simple to correct for these, so we first set $\sigma_{ex} = \sigma_{ey} = 0$. The correlation is very poor between the hard X-ray and FUV light curve (Fig. 2a), while the FUV and UVW1 are consistent with an almost perfect correlation with a lag of ~ 0.5 d (Fig. 2b). The correlation without considering the error bar variance is slightly worse between FUV and V band, while the lag is somewhat longer (Fig. 2c).

The neglect of the error bar variance can suppress the correlation, so we first investigate how much of the lack of correlation in Figs 2(a)–(c) is due to this. We assess the size of this effect by calculating the autocorrelation function (ACF). For an evenly sampled light curve with independent errors, the error bars are correlated only at zero lag, giving an additional spike at zero on top of the intrinsic ACF shape. The interpolated light curves have correlated errors on time-scales of the interpolation, so instead of a spike at zero lag, these form a component with width ~ 0.5 d on top of the intrinsic ACF. We show the ACF of the interpolated UVW1- and V-band light curves as the solid black lines in Figs 2(b) and (c), respectively. We do not show the ACF of the FUV lightcurve as this has such small errors and such good sampling that there is negligible error bar variance in this light curve. We fit the ACFs with two Gaussians: one broad Gaussian to model the intrinsic ACF and one narrow Gaussian to represent the correlated errors, both of which should peak at zero lag. This gives the value of σ_e^2 that must be subtracted in order for the broad Gaussian to peak at unity. For UVW1, we find that $\sigma_e^2 = 0.022\sigma_{\text{UVW1}}^2$, and for the V band, we find $\sigma_e^2 = 0.095\sigma_V^2$. We subtract this correlated error variance to get the error-corrected interpolated correlation function (Figs 2b and c, dashed red lines). The effect is quite small for the (already very good) FUV–UVW1 correlation, but makes a noticeable difference to the FUV–V band cross-correlation. The intrinsic variability in the V-band light curve is then consistent with an almost perfect correlation with the variable FUV light curve, but with an ~ 2 d lag (see also McHardy et al. 2014; Edelson et al. 2015; Fausnaugh et al. 2016).

In Fig. 2(a), we show the hard X-ray ACF (black line). It is not possible to apply the Gaussian fitting method to the hard X-ray ACF as the fast-varying hard X-rays show an intrinsic peak of correlated variability on ~ 0.5 d time-scales (Noda 2016) that cannot easily be separated from the effects of any correlated errors. However, we calculate the error bar variance of the hard X-ray light curve from the data and find that it is roughly $\sigma_e^2 \sim 0.013\sigma_X^2$. This is negligible and cannot explain the poor correlation shown by the hard X-ray–FUV CCF, indicating that the poor correlation between the hard X-ray and FUV light curves is intrinsic to the process.

3 LIGHT CURVES AND SPECTRA FROM BB DISC REPROCESSING HARD X-RAY EMISSION

Not all the irradiating flux will thermalize, as some part will be reflected. The reflection albedo depends on the ionization state of the disc, but for such a hard spectrum, it varies only from 0.3 (neutral) to 0.5 (completely ionized), giving $f_{\text{irr}} = 0.7$ –0.5. We choose $f_{\text{irr}} = 0.5$ in all subsequent models.

We first explore the scenario in Section 2, where a flared BB disc with a scaleheight of 0.1 on its outer edge extends inwards from the self-gravity radius at $r_{\text{out}} = 660$ down to 70, with the flow then forming a hot corona whose illumination can be approximated by a point source at height $h_x = 10$ above the black hole. The

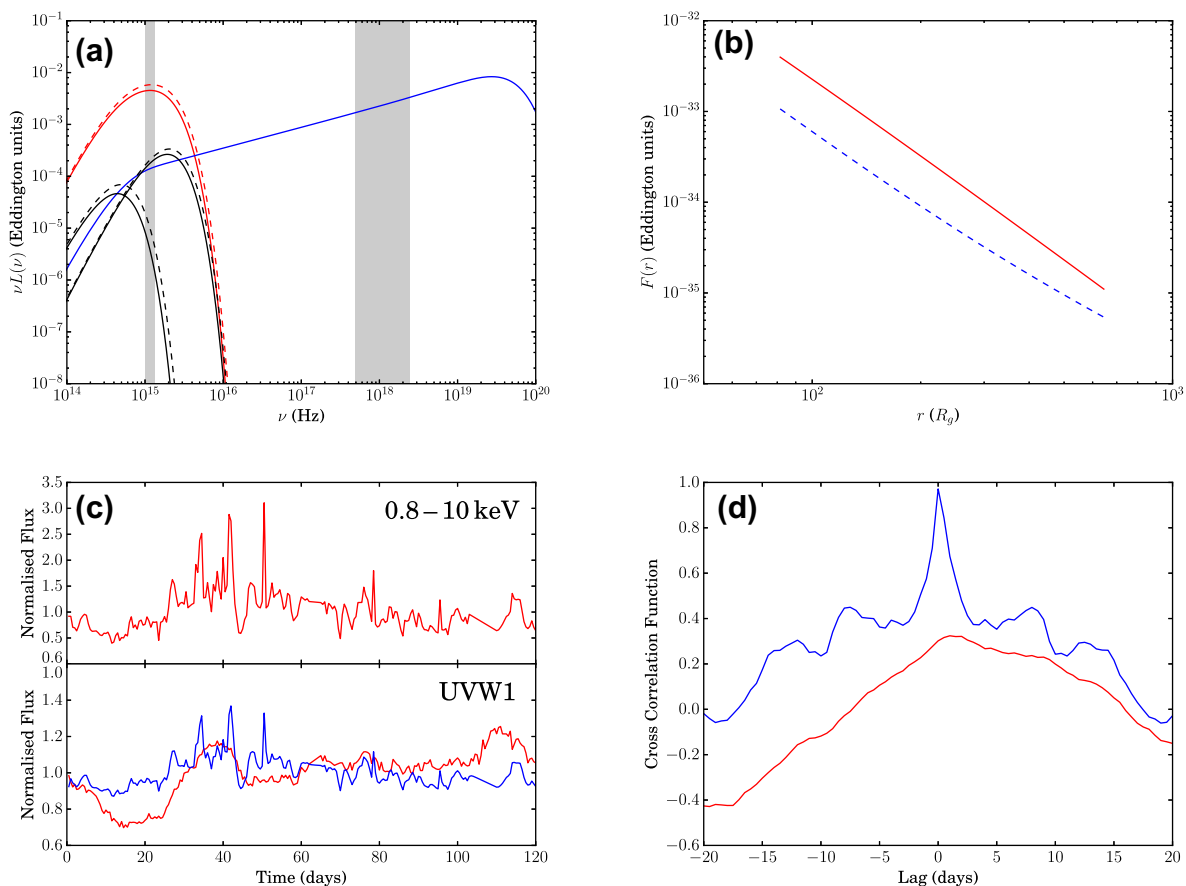


Figure 3. Standard BB disc with $r_{\text{cor}} = 70$ reprocessing hard X-ray emission. (a) Model spectrum: solid red line shows total intrinsic BB disc emission; dashed red line shows total disc emission including reprocessing; black lines show emission from outermost and innermost disc radii, with solid and dashed lines for intrinsic and intrinsic plus reprocessed emission, respectively; blue line shows the hard coronal power law; grey-shaded regions, from the left- to right-hand side, show the locations of the UVW1 band and the hard X-ray band, respectively. (b) Intrinsic BB disc flux as a function of radius (red line) compared with illuminating hard X-ray flux available for reprocessing (dashed blue line). (c) Top panel shows the observed hard X-ray light curve of NGC 5548 input into the model; bottom panel shows the observed simultaneous UVW1 light curve (red) compared with the simulated UVW1 light curve (blue). (d) CCF of the observed UVW1 light curve with respect to the observed hard X-ray light curve (red), and the simulated UVW1 light curve with respect to the observed hard X-ray light curve (blue). Positive lag values indicate the UVW1 band lagging behind the hard X-rays.

solid red line in Fig. 3(a) shows the intrinsic BB disc emission that results from gravitational heating alone. The dashed red line shows the total disc emission, including additional heating by the illuminating corona. For illustrative purposes, we also show the emission from two individual annuli in black, with the lower energy example corresponding to the emission from $r_{\text{out}} = 660$ and the higher energy example corresponding to the emission from the innermost disc radius at 70. Again, solid lines show the intrinsic emission from gravitational heating alone and dashed lines show the total emission, including reprocessing.

The dashed red line in Fig. 3(a) shows that reprocessing makes very little difference to the total BB disc luminosity. This is because the disc is dominated everywhere by the intrinsic emission (red solid line in Fig. 3b) rather than by reprocessing (blue dashed line in Fig. 3b), and even increasing f_{irr} to its maximum plausible value of 0.7 cannot overcome this. Reprocessing does have slightly more effect at larger radii (because the BB disc is flared), but the disc emission is dominated by the smallest radii.

So far, we have considered the steady-state or time-averaged spectrum. In order to know how fluctuations in the hard X-ray flux will produce changes in the UV/optical emission from the BB disc, we must quantify how well each disc radius can respond to and reproduce changes in the illuminating continuum. For each annulus in the disc, we calculate its transfer function following

Welsh & Horne (1991). This accounts for light travel time distances to different radii within the annulus and different azimuths within each radius. The transfer function, $T(r, \tau)$, for a given radius, r , describes what fraction of the reprocessed flux from that radius has a given time delay, τ , with respect to the illuminating continuum. The fluctuations in the reprocessed flux from a given annulus are then

$$F_{\text{rep}}(r, t) = \frac{f_{\text{irr}} \cos(n)}{4\pi(r R_g)^2} \int_{\tau_{\text{min}}}^{\tau_{\text{max}}} T(r, \tau) L_{\text{cor}}(t) d\tau. \quad (4)$$

This causes the effective temperature of the annulus to vary as

$$T_{\text{eff}}(r, t) = T_{\text{grav}}(r) \left(\frac{F_{\text{rep}}(r, t) + F_{\text{grav}}(r)}{F_{\text{grav}}(r)} \right)^{1/4}. \quad (5)$$

The fluctuations in a given spectral band (e.g. UVW1) are then the sum of the fluctuations in the emission from each annulus contributing flux to that band. Fluctuations in reprocessed flux change the relative contributions of individual annuli to the total band flux. An increase in reprocessed flux increases the temperature of the annulus. This both increases the luminosity of the annulus and shifts the peak of its BB spectrum to higher energies. This may shift the peak emission from smaller radii out of the bandpass and shift more of the emission from larger radii, which usually peak below the bandpass, to higher energies and so increase their contribution to

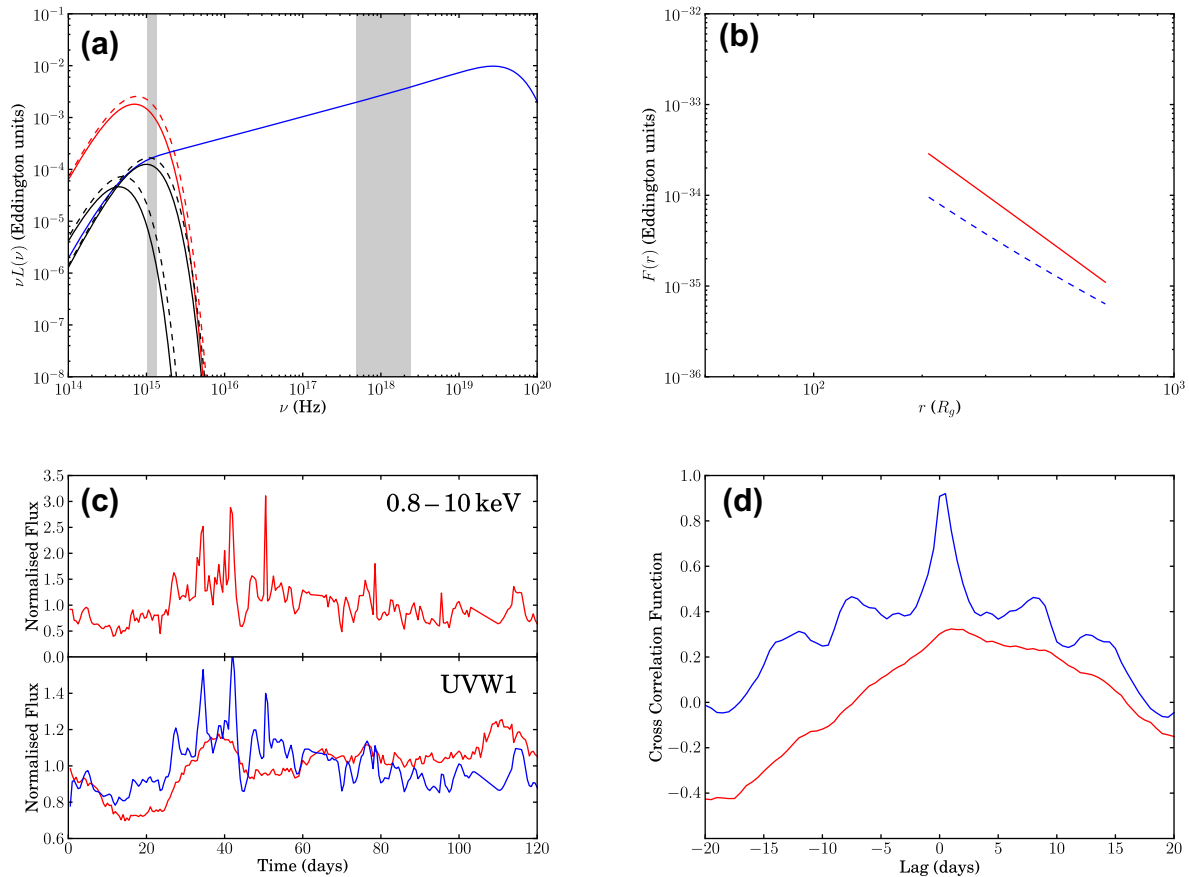


Figure 4. As in Fig. 3, but now for a standard BB disc with $r_{\text{cor}} = 200$ reprocessing hard X-ray emission.

the total band flux. As such, it is not appropriate to assume that a band is always dominated by emission from any one radius. By calculating the effective temperature and corresponding BB spectrum from each annulus at each time-step, our code accounts for this. We neglect any fluctuations in the intrinsic BB disc emission so that the only source of disc variability is the reprocessed fluctuations.

For our coronal power-law fluctuations, we use the hard X-ray light curve of NGC 5548 presented by Edelson et al. (2015), interpolated as described in the previous subsection to produce an evenly sampled input light curve with $dt = 0.5$ d. We input this into our disc reprocessing model and this allows us to calculate a model UVW1 light curve, which we can then compare to the observed data. We show our results in Fig. 3(c) (bottom panel), where the red line shows the observed UVW1 light curve and the blue line shows our predicted UVW1 light curve using this model. For reference, we also show the input hard X-ray light curve (top panel). Our simulated UVW1 light curve clearly fails to reproduce both the amplitude of fast variability (much more in the model than in the data) and the overall long-term shape of the observed UVW1 light curve (especially the dip in the observed light curve at 18 d and the rise at 110 d).

In Fig. 3(d), we show the CCF of the simulated UVW1 light curve with respect to the hard X-ray light curve (blue), compared to the CCF of the observed UVW1 light curve with respect to the hard X-ray light curve (red). A positive lag indicates the UVW1 band lagging behind the hard X-rays. The predicted CCF is strongly peaked with an almost perfect correlation at close to zero lag, and is quite symmetric. The observed CCF has none of the well-correlated, narrow components at lags < 1 d, but is instead quite poorly correlated,

and asymmetric with a peak indicating that the UVW1 band lags behind the hard X-rays by ~ 0.5 – 2 d (Edelson et al. 2015).

Clearly, this is not a viable model of the UVW1 light curve. The data require more reprocessing at longer lags, and less reprocessing at shorter lags. Certainly, the inner disc produces the shortest time lags, so truncating the BB disc at a larger radius could suppress some of the fast variability. We explore this in the next section.

3.1 Increasing disc truncation

We rerun our model with the BB disc truncated at a much larger radius, such that $r_{\text{cor}} = 200$. Such a large truncation radius for such a low mass accretion rate AGN is consistent with the observed trend in local AGN for r_{cor} to anticorrelate with L/L_{Edd} (Done et al. 2012; Jin et al. 2012). We show the results of using this larger truncation radius in Fig. 4. The key difference in the spectrum is that the hottest parts of the BB disc are no longer present, with the energy instead giving a slight increase in the normalization of the hard X-ray Comptonization component. The small disc component gives a significantly lower UVW1 flux, so the variable components from both the direct Comptonization component and its reprocessed UV flux now contribute a higher fraction of the UVW1 band.

The model can now better reproduce the observed amplitude of UVW1-band long-term flux variations (blue light curve in Fig. 4c, especially the dip at 18 d). However, our simulated UVW1 light curve still has much more fast variability than is seen in the real UVW1 light curve. The simulated UVW1 light curve clearly looks like the hard X-ray light curve from which it was produced. Yet the

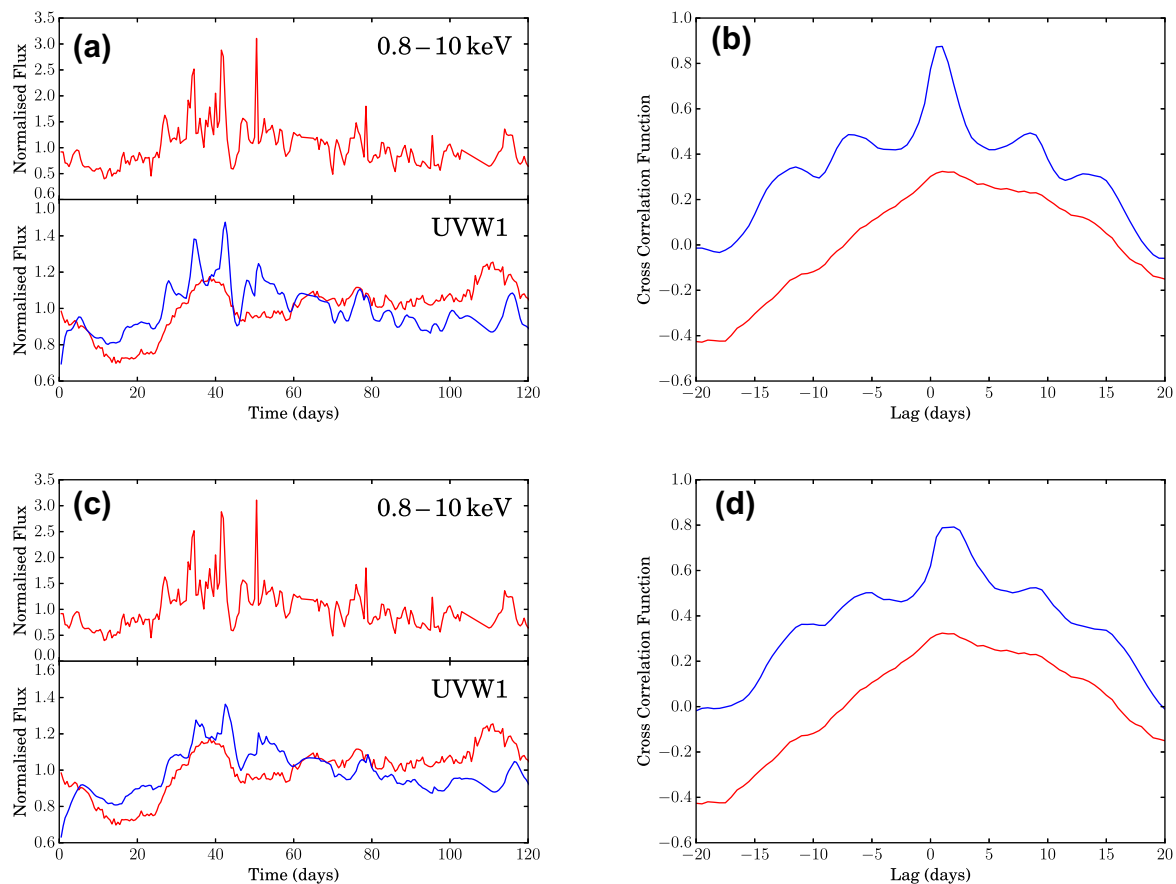


Figure 5. BB disc with $r_{\text{cor}} = 200$ reprocessing hard X-ray emission but with reprocessing coming from a larger effective radius. (a) and (b): comparison of the simulated UVW1 light curve and CCF (blue) with the observations (red) for an effective reprocessing radius twice that expected from a standard BB disc. (c) and (d): comparison of the simulated UVW1 light curve and CCF (blue) with the observations (red) for an effective reprocessing radius four times that expected from a standard BB disc.

observed UVW1 light curve looks quite different from the observed hard X-ray light curve.

This is shown clearly in Fig. 4(d) where we compare the CCFs. The CCF peak from our simulated light curve has shifted to ~ 0.5 d rather than the close to zero-peaked CCF of the previous model, but the lag is still not as long as in the observed CCF, and the model UVW1 light curve is much more correlated with the hard X-ray light curve. This is seen at all lags, but the problem is especially evident on short lag times, showing quantitatively that the model UVW1 light curve has much more of the fast variability seen in the hard X-ray light curve than the real data.

Edelson et al. (2015) commented that the lags they measure are much longer than expected from reprocessing on a standard BB disc, i.e. the radii that should show peak emission in the UVW1 band are much smaller than the radii implied by the light travel time delayed response of emission in that band. This would suggest that the accretion disc around NGC 5548 is not a standard BB disc. Somehow, the same emission is produced at a larger radius than standard BB disc models predict.

We test this by altering our disc transfer functions such that the reprocessing effectively occurs at twice (Figs 5a and b) and then four times (Figs 5c and d) the radius at which a standard BB disc would produce that emission. In theory, this should improve our simulated light curves, as reprocessing at larger radii smooths out fast fluctuations, so it should reduce the amount of high-frequency power in the light curve.

However, Fig. 5(a) shows that an effective radius twice that of a standard BB disc does not smooth the simulated light curve enough. An effective radius four times that of a standard BB disc does a better job (Fig. 5c), but comparison of the CCFs (Fig. 5d) illustrates that this is still not a good match to the data. An effective radius four times that of a standard BB disc may be required to sufficiently reduce the high-frequency power in the light curve, but this then gives light travel time lags that are too long. The peak lag of the observed CCF is roughly 0.5–2 d, while the peak lag from the model light curve extends from ~ 1 to 3 d. The observed smoothing time-scale is much longer than the lag time-scale, and this cannot be replicated by light travel time smoothing, as light travel time effectively ties the smoothing to the lag time-scale. For this reason, doubling the black hole mass to match the Bentz et al. (2010) estimate does not solve the problem of transmitting too much high-frequency power into the optical. Increasing the disc inclination angle increases the amount of smoothing; however, this effect is negligible even when setting $i = 75^\circ$ (an unreasonably large angle for a Seyfert 1 such as NGC 5548) and likewise cannot reduce the high-frequency power in the model optical light curves.

Moreover, the model light curves are all far more correlated with the hard X-ray light curve, on all time-scales, than the observed light curve is. Even in Fig. 5(d), the peak correlation coefficient between the hard X-rays and the model UVW1 light curve is ~ 0.8 , while between the hard X-rays and the observed light curve, it is only ~ 0.3 .

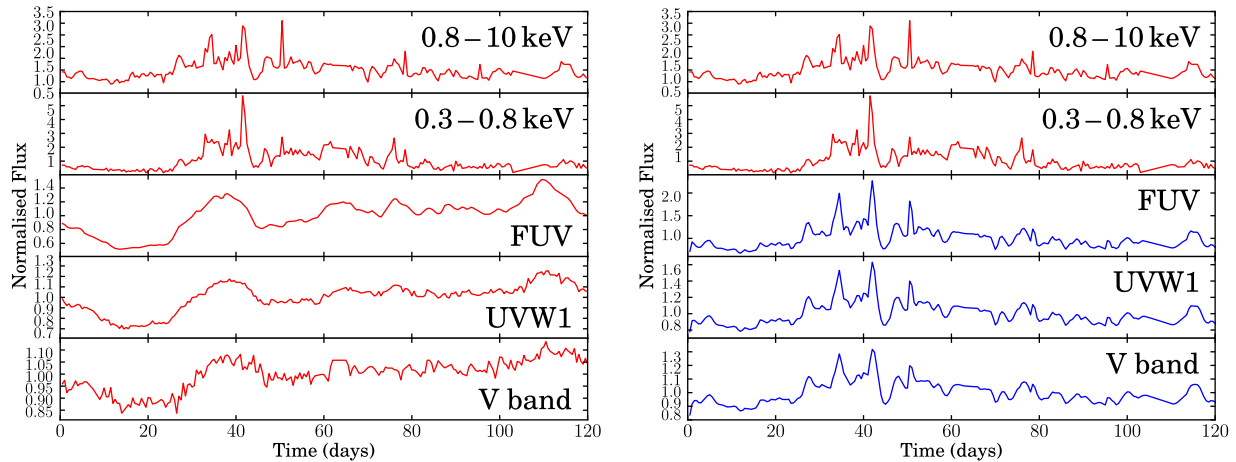


Figure 6. Left-hand panel: observed simultaneous hard X-ray, soft X-ray, FUV, UVW1 and V-band light curves of NGC 5548. Right-hand panel: observed simultaneous hard X-ray (input into the model) and soft X-ray light curves of NGC 5548, together with resulting FUV, UVW1 and V-band light curves simulated by the model with a standard BB disc with $r_{\text{cor}} = 200$ reprocessing hard X-ray emission.

Fig. 6 further illustrates this. In the left-hand panel, we show the observed light curves – from the top to bottom – for hard X-rays, soft X-rays, FUV, UVW1 and V band. In the right-hand panel, we again show the observed hard and soft X-ray light curves, followed by our model FUV, UVW1 and V-band light curves using the standard BB disc model. It is clear that reprocessing the hard X-ray light curve off a standard BB disc size limited by the self-gravity radius produces UV and optical light curves that look like the original hard X-ray light curve. The hard X-ray flares (e.g. at 42 d) are slightly more smoothed in the longer wavelength bands, but they are still clearly recognizable.

In contrast, the observed UV and optical light curves lack any short-term flares and show additional longer time-scale variability that is not present in the hard X-ray light curve (e.g. the dip between ~ 10 and 30 d). The FUV-to-V-band light curves are clearly well correlated with one another, with peak CCFs with respect to the FUV of 0.7–0.9 (Edelson et al. 2015), and the increasing lags with increasing wavelength suggest that reprocessing is a key linking factor. But they are much less well correlated with the hard X-rays (with a peak CCF of only ~ 0.3). The left-hand panel of Fig. 6 shows that there is a clear break in properties between the observed X-ray and UV–optical light curves. The right-hand panel shows that, if the hard X-rays are the source of illuminating flux, this cannot occur.

There are really only two ways out of this impasse: Either the hard X-ray light curve is not a good tracer of the illuminating flux or the BB accretion disc is shielded from being illuminated by the hard X-rays. The former is plainly a possibility, as the hard X-ray light curve from 0.8 to 10 keV is not at the peak of the hard X-ray emission, and Noda et al. (2011) show that there can be a fast-variable steep power-law component. Mehdipour et al. (2015) and Ursini et al. (2015) show that the hard X-ray variability encompasses a change in both normalization *and* spectral index, with the spectrum softening as the source brightens. A hard X-ray light curve at 100 keV would be a better direct tracer of the total hard X-ray flux, but until this is available, we estimate this using the intrinsic power-law spectral index and normalization derived by Mehdipour et al. (2015). These are binned on 10-d intervals to get a sufficient signal-to-noise ratio, so it is not a sensitive test of the model, but assuming that the spectral cut-off remains fixed at 100 keV, this still does not give a good match to the FUV light curve. We conclude that it is more likely that the reprocessing region is

shielded from the hard X-ray illumination, and consider below how this might also shed light on the origin of the soft X-ray excess.

4 LIGHT CURVES AND SPECTRA FROM BB DISC REPROCESSING FUV EMISSION

The broad-band spectrum of NGC 5548 presented by Mehdipour et al. (2015) shows that a two-component BB disc + hard power-law model is clearly not sufficient to fit its spectrum. This source shows a strong soft X-ray excess above the 2–10 keV power law, which can be well fitted with an additional low-temperature, optically thick Compton component, though this is not a unique interpretation. It can also be well fitted in the 0.3–10 keV bandpass with highly smeared, partially ionized reflection (Crummey et al. 2006). However, with the advent of NuSTAR and other high-energy instruments, it is now clear that the reflection interpretation does not give such a good fit to the data up to 50–100 keV for AGN with hard X-ray spectra (e.g. Boissay et al. 2014; Matt et al. 2014). Hence, we assume that the optically thick Compton component, which produces the soft X-ray excess, is an additional intrinsic continuum component.

To include this, we now assume that the BB disc truncates at r_{cor} as before, but that the remaining gravitational power inwards of this radius is split between two coronal components: the hard power law and the optically thick Compton component. We fix the temperature and optical depth of the optically thick Compton component to $kT_e = 0.17$ keV and $\tau = 21$ (Mehdipour et al. 2015). This component then peaks in the UV as required by the spectrum. By reducing the fraction of coronal energy in the hard power law to $f_{\text{pl}} = 0.75$, i.e. 0.25 of the coronal energy goes instead into powering the optically thick Compton component, we are again able to match the ratio of $F_{\text{UVW1}}/F_{10\text{keV}} \sim 1.7$ found by Mehdipour et al. (2015), with $r_{\text{cor}} = 200$, which we could not do previously with a substantially truncated disc and no optically thick Compton component. In Fig. 7(a), we show this new model spectrum, with the optically thick Compton component shown in green.

While the origin of this emission is not well understood, it is clearly not from a standard disc. This component takes over from the standard BB disc in the UV, which may not be a coincidence as the substantial atomic opacity in the UV can cause changes in the disc structure compared to a Shakura–Sunyaev disc that

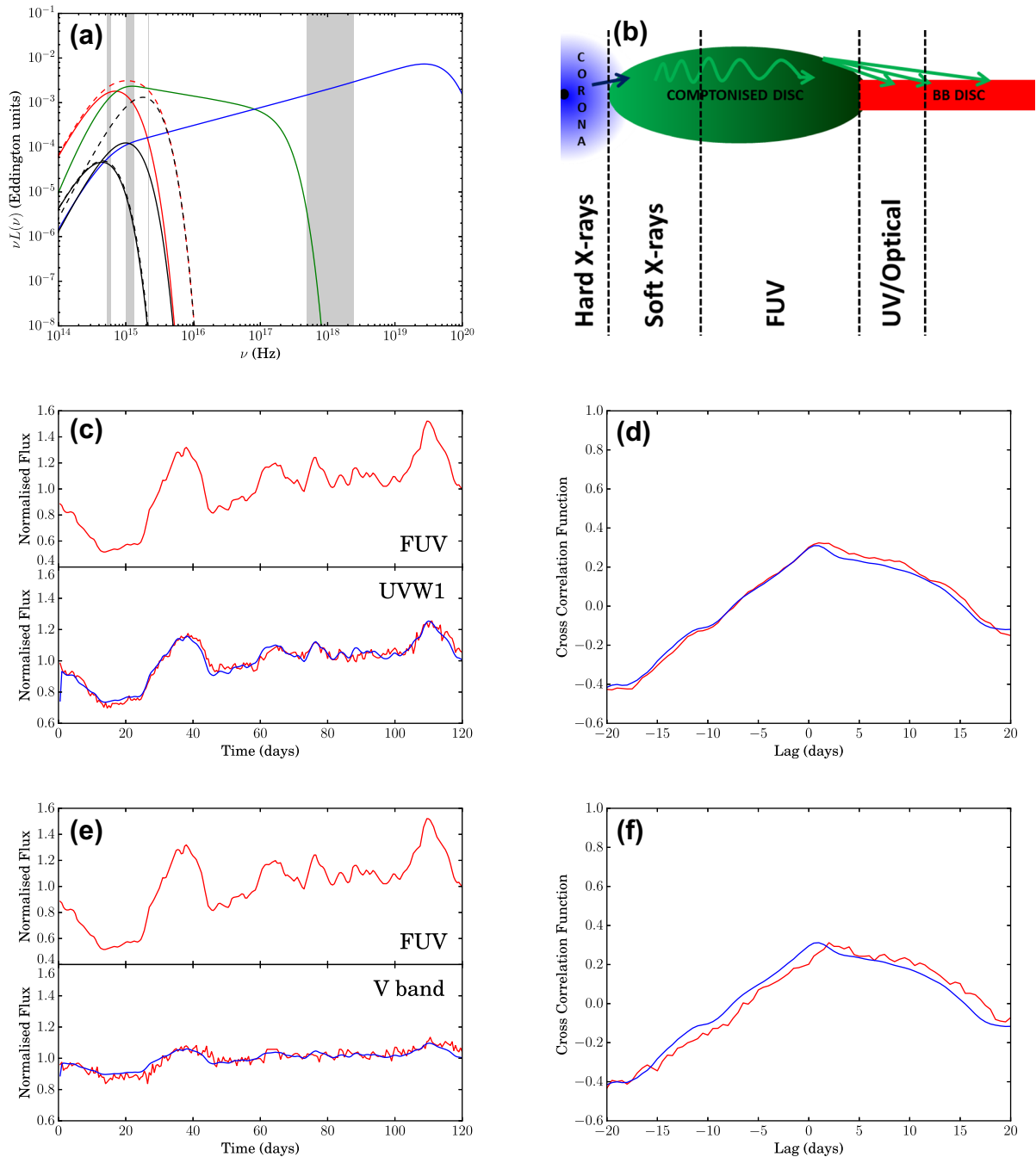


Figure 7. Standard BB disc plus Comptonized disc component, with $r_{\text{cor}} = 200$ and BB disc reprocessing FUV emission. (a) Model spectrum: solid red line shows total intrinsic BB disc emission; dashed red line shows total BB disc emission including reprocessing; black lines show emission from outermost and innermost BB disc radii, with solid and dashed lines for intrinsic and intrinsic plus reprocessed emission, respectively; green line shows the optically thick Compton component from the Comptonized disc; blue line shows hard coronal power law; grey-shaded regions, from the left- to right-hand side, show the locations of the V band, UVW1 band, FUV band and hard X-ray band, respectively. (b) Cartoon of a scenario where the Comptonized disc obscures the inner hard X-ray region and is instead the source of flux illuminating the outer BB disc. Dashed lines suggest transitions between regions of material producing the bulk of the emission in a given band. (c) The top panel shows the observed FUV light curve of NGC 5548 input into the model; bottom panel shows the observed simultaneous UVW1 light curve (red) compared with the simulated UVW1 light curve (blue). (d) CCF of the observed UVW1 light curve with respect to the observed hard X-ray light curve (red), and the simulated UVW1 light curve with respect to the observed hard X-ray light curve (blue). Positive lag values indicate the UVW1 band lagging behind the hard X-rays. (e) and (f): same as (c) and (d) but for observed and simulated V-band light curves.

incorporates only plasma opacities of electron scattering and free-free absorption. In particular, UV line driving has the potential to lift the disc photosphere (e.g. Laor & Davis 2014). The copious hard X-ray emission in this object should quickly overionize any potential UV-line-driven wind, which would result in the material falling

back down again without being expelled from the system. This scenario has the potential to effectively increase the scaleheight of the disc, thus decreasing its density (Jiang, Davis & Stone 2016). This decreases its true opacity, hence increasing the effective colour-temperature correction (e.g. Done et al. 2012). Alternatively, UV

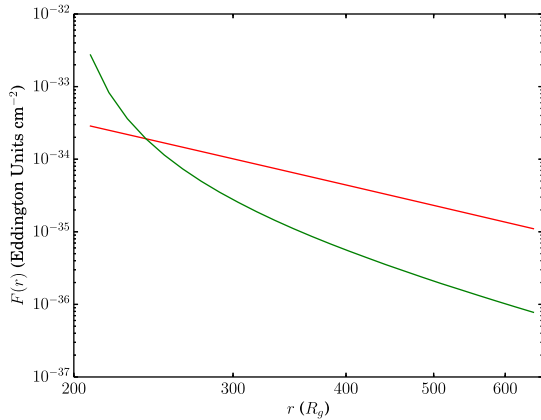


Figure 8. Illuminating FUV flux as a function of BB disc radius (for a flat disc) assuming that the FUV flux is emitted by a wall of material of height $10R_g$ located at $200R_g$ (green line). The red line shows gravitational flux dissipation of the BB disc.

temperatures are also linked to the onset of the dramatic disc instability connected to hydrogen ionization (Lasota 2001; Hameury, Viallet & Lasota 2009; Coleman et al. 2016). Whatever the origin, the total optical depth of the disc to electron scattering at the UV radii is probably of the order of 10–100 (Laor & Netzer 1989), so the optically thick Compton emission in this picture is coming from the disc itself, with the emission not quite able to thermalize to standard BB emission because of the increased scaleheight of the disc due to the UV radiation pressure and/or the onset of the hydrogen ionization instability. We therefore refer to the optically thick Compton component as the ‘Comptonized disc’, to distinguish it from the outer BB disc.

The break in properties between the soft X-ray and FUV light curves shows clearly that the Comptonized disc is itself stratified rather than being a single spectral component as in Mehdipour et al. (2015). We show our potential geometry in Fig. 7(b), where the soft X-ray emission comes from the inner regions of this large scaleheight flow, which still cannot illuminate the outer BB disc, while the FUV is produced at larger radii and can illuminate the outer BB disc.

We model this FUV illumination by assuming a cylinder of material located at a particular radius ($r_{\text{irr}} > 0$), with a particular height (h_{max}). This changes the illumination pattern, so we can no longer use the approximation of an on-axis point source. We calculate the reprocessed flux at a given BB disc radius by dividing the ‘surface’ of the wall into elements (azimuthally – $d\phi$ – and vertically – dh) and summing the flux contribution from each element:

$$F_{\text{rep}}(r) = \int_0^{h_{\text{max}}} \int_0^{2\pi} \frac{f_{\text{irr}} L_{\text{cor}}}{2\pi^2 h_{\text{max}} R_g^2} \frac{h dh d\phi}{(r^2 + r_{\text{irr}}^2 + h^2 - 2r_{\text{irr}} r \cos \phi)^{3/2}}. \quad (6)$$

This new illumination pattern intensifies the illumination on radii close to r_{irr} but for $r \gg r_{\text{irr}}$, it becomes indistinguishable from the case of a lamppost point source. We set $r_{\text{irr}} = r_{\text{cor}}$ and $h_{\text{max}} = 10$, implying a scaleheight for the outer edge of the Comptonized disc of $h/r = 0.05$, which should be sufficient to obscure the hard X-ray emission. The resulting illumination profile is shown in Fig. 8 (green line).

In Figs 7(c) and (d), we compare the resulting model UVW1 light curve with the observations. We now find a much better match to the behaviour of the observed UVW1 light curve, matching the

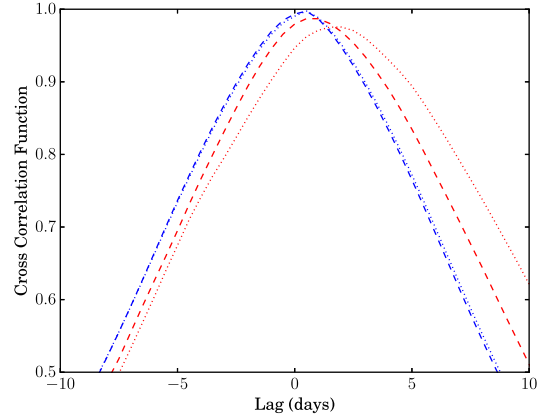


Figure 9. Comparison of CCFs with respect to the FUV for the standard BB disc plus Comptonized disc FUV reprocessing model. Dashed lines show CCF of UVW1 with respect to FUV, and dotted lines show CCF of the V band with respect to FUV. Red lines show CCFs calculated using the observed light curves, while blue lines show the corresponding CCFs calculated using the simulated light curves.

amplitude of fluctuations and reproducing the shape of the UVW1/hard X-ray CCF.

In Figs 7(e) and (f), we also compare our model V-band light curve with the data. We find a good match to the amplitude of the observed fluctuations, but the model V-band CCF with respect to the hard X-rays (blue) is not lagging by as much as the real V-band light curve (red). This mismatch is more evident when comparing the model UVW1 and V-band CCFs with respect to the FUV. Fig. 9 shows that both the model UVW1 (blue dashed) and V-band (blue dotted) CCFs with respect to the FUV peak at close to zero lag, while the real UVW1 (red dashed) and V-band (red dotted) CCFs are significantly shifted away from zero lag.

Thus, while reprocessing the FUV gives light curves that are a much better match to the data, the response of our model light curves is too fast. The observed V-band lag behind the FUV light curve is ~ 2 d (Edelson et al. 2015). For a black hole mass of $3.2 \times 10^7 M_{\odot}$, this means that the reprocessed V-band flux must be emitted roughly $1080R_g$ away from wherever the FUV emission occurs. The observed UVW1 lag is ~ 0.5 d, implying that it is emitted at a distance of $\sim 270R_g$ from the FUV emission. In our model, we assume that the FUV emission is supplied by the outer edge of the Comptonized disc at $\sim 200R_g$. However, regardless of the exact location of the FUV emission, the observed light curves imply that the reprocessed V-band flux must be emitted $\sim 700R_g$ further away from the FUV continuum than the reprocessed UVW1 flux. So far, we have used a BB disc truncated at the self-gravity radius of $660R_g$ as our reprocessor. Clearly, this does not provide a large enough span of reprocessing radii. We now rerun our model with a larger outer radius for the BB disc, to see if we can reproduce the observed length of the V-band lag.

4.1 Increasing outer disc radius

We increase the outer radius of the BB disc to $2000R_g$ and rerun our FUV reprocessing simulation. We find that increasing the outer radius of the BB disc makes no difference to the length of our simulated V-band lag. Fig. 10 illustrates why.

A 2-d V-band lag requires the V band to be dominated by reprocessed flux emitted from $R = 2ld > 1000R_g$ (for a $3.2 \times 10^7 M_{\odot}$ like NGC 5548). Fig. 10 shows that BB disc annuli at these large

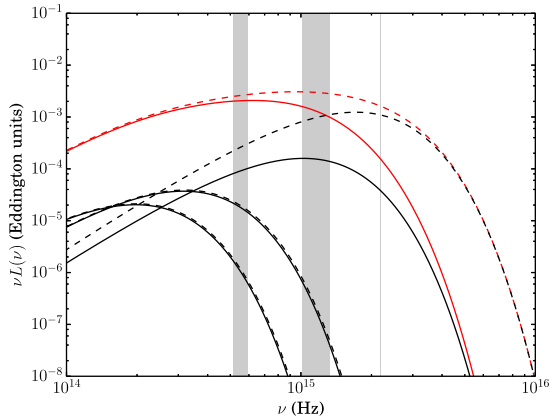


Figure 10. Disc spectrum from the standard BB disc reprocessing FUV emission model with $r_{\text{cor}} = 200$ and r_{out} increased to 2000. The solid red line shows total intrinsic BB disc emission; dashed red line shows total BB disc emission including reprocessing; pairs of black lines from the left- to right-hand side show emission from the outermost radius, an intermediate radius ($r = 1000$) and the innermost radius of the BB disc, with solid and dashed lines showing intrinsic and intrinsic plus reprocessed emission, respectively. Grey-shaded regions, from the left- to right-hand side, show the locations of the V band, UVW1 band and FUV band, respectively.

radii are simply too cool to contribute significant flux to the V band. This is due to their large area. Illumination by the FUV continuum simply cannot raise their temperature enough to make them contribute significantly to the V band, let alone dominate its flux. The dashed lines in Fig. 10 show how little the illumination increases the total BB disc flux at these very large radii.

The amount of FUV flux intercepted by large disc radii can be increased by increasing the BB disc flaring, i.e. by increasing $h_{\text{out}}/r_{\text{out}}$. The larger the outer disc scaleheight is, the more illuminating flux the annulus intercepts, the greater the heating is and the more V-band flux it contributes. We set $h_{\text{out}}/r_{\text{out}} = 0.5$ but this produces a negligible increase. The heating flux is simply spread over too large an area.

In order for a reprocessor located at 2 light-days ($R > 1000R_g$) to contribute significant V-band flux, it must have a small area. Clearly

disc annuli are not suitable for this, since the area of the annulus is constrained to scale with its radius as $A(dr) \sim 2\pi R dr$. An obvious source of small-area reproducers at large radii is the BLR clouds. In the next section, we investigate the possibility that the observed optical lags are due to reprocessing of the FUV emission, not by a BB disc, but by BLR clouds.

4.2 BLR clouds reprocessing FUV emission

BLR clouds absorb UV continuum emission and re-emit the energy as optical lines/recombination continua. Clearly, these do contribute to the observed flux, and are lagged by the size scale of the BLR. We first explore if this contamination by the BLR can influence the lags, as suggested by Korista & Goad (2001).

Mehdipour et al. (2015) show the UV/optical spectrum taken during the campaign. We reproduce this in Fig. 11(a) (Mehdipour, private communication), with the continuum bands superimposed. The UVW1 band contains a substantial amount of blended Fe II and Balmer continuum (Fig. 11a, magenta line) as well as a broad Mg II emission line (Fig. 11a, blue line). The strongest line contribution to the V band comes from the narrow [O III] emission line (Fig. 11a, blue line), with a small contribution from the wing of H β .

We conduct a simple test to determine whether this BLR line contamination could explain the observed optical lags. The FUV is dominated by continuum emission, so we assume that the continuum component varies as the FUV light curve, so that there are no real continuum lags. H β lags the continuum in this source by roughly 15 d (Peterson et al. 2002), though this does change with flux, spanning 4–20 d (Cackett & Horne 2005; Bentz et al. 2010). We assume that all the BLR emission components (eg. Fe II/Balmer blend, Mg II and H β) are a lagged and smoothed version of the FUV light curve, where the lag and smoothing time-scale is 15 d, while the narrow [O III] emission line is constant on the time-scale of our observations. Finally, we dilute this by the required amount of constant host galaxy component (Mehdipour et al. 2015) to get the full spectrum as a function of time. Integrating this over the UVW1 and V bands gives the simulated light curves for this model. Fig. 11(b) shows the CCFs of these with respect to the FUV-band light curve (blue), in comparison with the CCFs of the real light

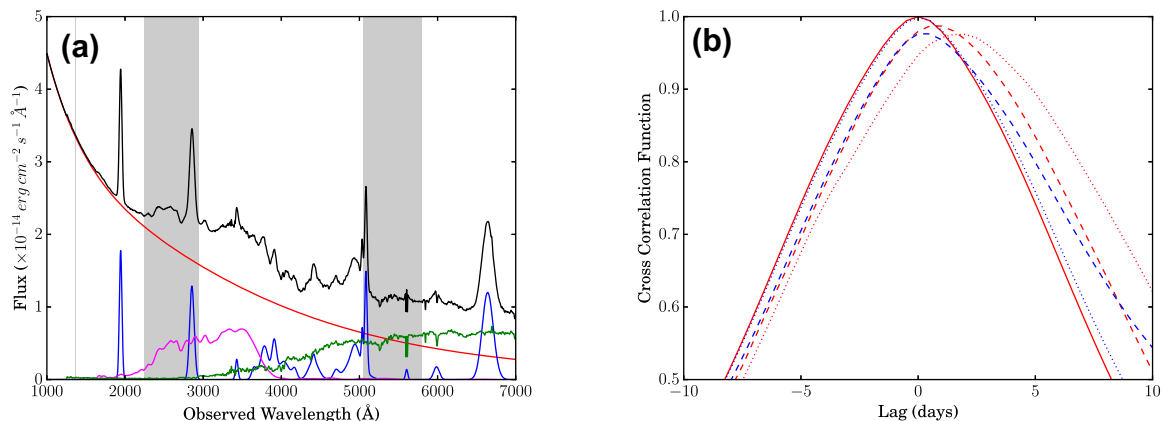


Figure 11. Model assuming that line emission is the only source of reprocessed emission. (a) UV/optical spectral fit for NGC 5548 from Mehdipour et al. (2015), together with their spectral decomposition. The red line shows continuum emission, blue shows broad- and narrow-line components, magenta shows blended Fe II with Balmer continuum, green shows host galaxy contribution and black shows the resulting total spectrum. Grey-shaded regions, from the left- to right-hand side, show the locations of the FUV, UVW1 and V bands, respectively. (b) Comparison of CCFs for the model assuming that line emission is the only source of reprocessed emission. The solid line shows the CCF of FUV with respect to FUV (i.e. autocorrelation), dashed lines show the CCF of UVW1 with respect to FUV and dotted lines show the CCF of the V band with respect to FUV. Red lines show CCFs calculated using the observed light curves, while blue lines show the corresponding CCFs calculated using the simulated light curves.

curves (red), with the UVW1 band as the dashed lines, and the *V* band as dotted lines. The red solid line shows the CCF of the FUV light curve with itself, i.e. the FUV ACF.

Both model CCFs peak at zero, whereas the observed CCFs have peaks offset from zero. This is because the flux contribution from broad lines is simply not large enough to shift the CCF peaks away from zero in either UVW1 or the *V* band. Furthermore, UVW1 contains more broad-line contamination than the *V* band, and as a result, the UVW1 model CCF (blue dashed line) is more positively skewed than the *V*-band CCF, which is almost identical to the FUV ACF (compare blue dotted and red solid lines). This is in clear contrast to the data, where the *V*-band light curve contains less line contamination than UVW1 and yet shows a longer lag than UVW1. The UVW1 and *V*-band lags therefore cannot be explained through contamination by lagged broad-line emission.

5 THERMAL REPROCESSING

So far, we have worked forward from a geometric model of the spectrum and its reprocessed emission, then calculated the resulting timing properties and compared these to the observations. Now we take the opposite approach. We begin by matching the timing properties of the source (specifically the light-curve amplitudes and CCFs) and use these to infer the spectral components and then the geometry.

We begin by matching the shape of the UVW1 and *V*-band CCFs. The peak lag (i.e. the lag at which the CCF is a maximum) of the observed UVW1 light curve with respect to the observed FUV light curve is ~ 0.5 –1 d. The CCF of the FUV light curve with respect to itself (i.e. the FUV autocorrelation) peaks at zero, as there is no lag between the two light curves. The CCF of the FUV light curve lagged and smoothed by 1 d with respect to the original FUV light curve will peak at 1 d. This is not the only way a CCF peak at 1 d can be produced. If a light curve consists of equal-amplitude contributions from two light curves, one of which is the original unlagged FUV light curve and the other is the FUV light curve lagged and smoothed by 2 d, then the CCF of this composite light curve with respect to the original FUV light curve will be the sum of the two CCFs – the unlagged FUV with respect to itself and the 2-d-lagged FUV with respect to the unlagged FUV – so that the resulting CCF will peak, not at 0 or 2 d, but at 1 d. More generally, any composite light curve CCF will be the sum of the component light curve CCFs weighted by the fraction of the total band flux coming from each light curve that is correlated with the reference light curve. In this way, we can constrain the flux contributions of variable components with different lags to a given band by matching the peak and shape of the CCF.

We use 16 variable component light curves: the original FUV light curve, the FUV light curve lagged and smoothed by 1 d, the FUV light curve lagged and smoothed by 2 d, the FUV light curve lagged and smoothed by 3 d, etc., up to a maximum lag of 15 d. We then combine these component light curves to simulate model UVW1 and *V*-band light curves and then compare the CCFs of these model light curves to the observed CCFs. We systematically adjust the component light-curve contributions and select the fractional contributions that produce the smallest difference (Δ) between model and observed CCFs, where
$$\Delta = \sum_{\tau=-20\text{d}}^{\tau=+20\text{d}} |\text{CCF}_{\text{UVW1,obs}}(\tau) - \text{CCF}_{\text{UVW1,model}}(\tau)| + \sum_{\tau=-20\text{d}}^{\tau=+20\text{d}} |\text{CCF}_{\text{V,obs}}(\tau) - \text{CCF}_{\text{V,model}}(\tau)|.$$
 Since UVW1 and the *V* band are spectrally close (and the BBs we will fit to the components are broad in comparison), we require both bands to contain the

Table 1. Light-curve fractions from model fits to the observed UVW1 and *V*-band CCFs shown in Fig. 12. f_{FUV} is the fraction of total band flux contributed by the unlagged FUV light curve. $f_{\text{FUV}-6\text{d}}$ is the fraction of total band flux contributed by the FUV light curve lagged and smoothed by 6 d. f_c is the fraction of total band flux that is constant. There are two possible sources of constant flux: intrinsic BB disc emission (f_d) and the host galaxy (f_g), such that $f_d + f_g = f_c$.

	UVW1	<i>V</i> band
f_{FUV}	0.395	0.189
$f_{\text{FUV}-6\text{d}}$	0.105	0.111
f_c	0.500	0.700
f_d	0.500	0.350
f_g	0.000	0.350

same lagged components (although the fractional contributions of these components in each band will differ).

We find that the best-fitting model under these constraints requires UVW1 and the *V* band to contain a contribution from the original FUV light curve, plus a contribution from the FUV light curve lagged and smoothed by 6 d. Table 1 lists the corresponding fractional contributions (f_{FUV} and $f_{\text{FUV}-6\text{d}}$), while Fig. 12(a) shows the resulting model CCFs (blue), compared to the observed CCFs (red), where UVW1 CCFs are shown with dashed lines and *V*-band CCFs are shown with dotted lines. The model *V*-band CCF peaks at 1.5–2 d, in agreement with the data. The UVW1 CCF peaks at 0.5 d, again in agreement with the data.

Matching the CCFs allows us to constrain the lagged, i.e. variable, flux contributions to the UVW1 and *V* bands. If the UVW1 and *V* bands contained only these variable components, then they would have equal-amplitude fluctuations. The observed FUV, UVW1 and *V*-band light curves shown in Fig. 12(b) in solid, dashed and dotted red lines, respectively, clearly do not have equal amplitudes. The amplitude decreases with increasing wavelength, implying that the fluctuations are being increasingly diluted by a constant component. Matching the amplitude of our simulated UVW1 and *V*-band light curves to the observations allows us to constrain the fractional contribution of this constant component (f_c) to each band.

In reality, this constant component has two possible sources: intrinsic BB disc flux and flux from the host galaxy. The spectral decomposition in Mehdipour et al. (2015) (Fig. 11a) shows that the contribution of the host galaxy to the UVW1 band is negligible; hence, we can assume that all the constant flux in the UVW1 band is supplied by intrinsic BB disc emission (i.e. $f_d = f_c$, $f_g = 0$). In contrast, the spectrum in Mehdipour et al. (2015) shows that the flux contributions of the intrinsic BB disc continuum and the host galaxy are roughly equal in the *V* band, i.e. $f_d = f_g = f_c/2$. Each band therefore has contributions from a maximum of six spectral components, with the proportions of each listed in Table 1.

Having established the flux contributions of each temporal component to each band, we can now begin finding spectral components that can provide these flux levels in each band.

We begin with intrinsic BB disc emission. We introduce a standard BB disc (red line, Fig. 13), truncated at $r_{\text{in}} = 200$ with $\log L/L_{\text{Edd}} = -1.4$, as is required by the energetically constrained spectral decomposition shown in Fig. 7(a). This is the sole provider of constant flux in the UVW1 band. Since we know the fractional contribution of constant flux to the UVW1 band ($f_c = f_d = 0.5$; Table 1), this tells us that the total UVW1-band

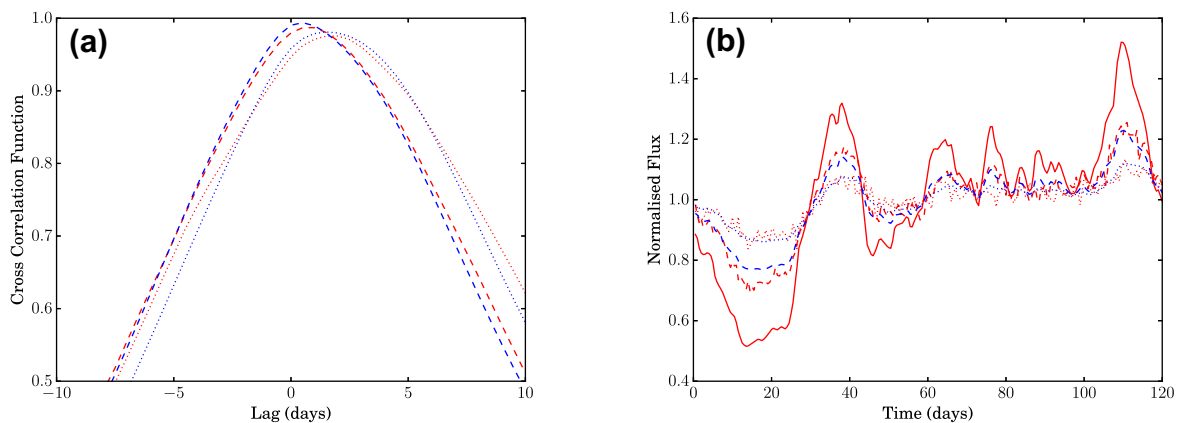


Figure 12. Best-fitting thermal reprocessing model using observed CCFs and light curves to constrain reprocessor flux contributions and reprocessor properties. (a) Comparison of CCFs. Dashed lines show the CCF of UVW1 with respect to FUV and dotted lines show the CCF of the V band with respect to FUV. Red lines show CCFs calculated using the observed light curves. Blue lines show the corresponding model CCFs using the simulated UVW1 and V-band light curves generated from the best-fitting component fractions listed in Table 1. (b) Comparison of observed light curves (red) with simulated light curves (blue) generated using the component fractions listed in Table 1. The solid line shows the observed FUV light curve. Dashed lines show UVW1 light curves and dotted lines show V-band light curves.

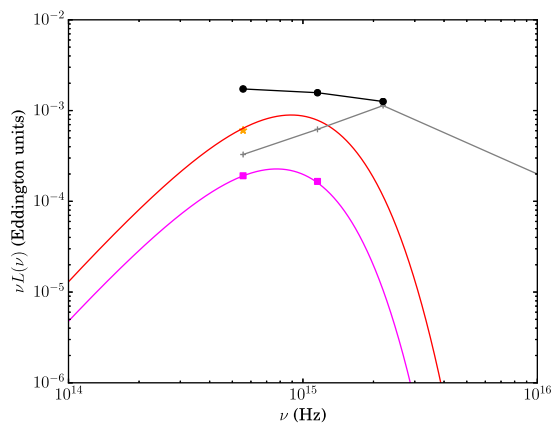


Figure 13. Spectral decomposition inferred from the component fractions listed in Table 1, which are shown to reproduce the observed timing properties of NGC 5548 in Fig. 12. The red line shows intrinsic (constant) emission from a BB disc truncated at $r_{\text{in}} = 200$, with $r_{\text{out}} = 300$. Black points, from the left- to right-hand side, show total flux in the V, UVW1 and FUV bands, respectively. The orange star shows the galaxy flux contribution to the V band. Grey crosses mark the inferred flux levels of the spectral component varying as the FUV light curve. Magenta squares mark the inferred flux levels of the variable component with a 6-d lag with respect to the FUV light curve, while the magenta line shows the corresponding BB spectrum that matches these flux levels. The distance, temperature and covering factor of this BB component are $R = 3240R_g$, $T = 9600$ K and $f = 0.002$.

flux is $F_{\text{UVW1}} = F_d(\nu_{\text{UVW1}})/f_d$ (central black point, Fig. 13). From figs 6(a) and (b) in Mehdipour et al. (2015), we can derive the ratio of dereddened FUV flux to UVW1 flux ($\nu F(\nu)_{\text{FUV}} \sim 0.8\nu F(\nu)_{\text{UVW1}}$), and the ratio of (dereddened but still including host galaxy) V-band flux to UVW1 flux ($\nu F(\nu)_{\text{Vband}} \sim 1.1\nu F(\nu)_{\text{UVW1}}$). From our total UVW1 band flux, we can therefore calculate the total FUV and total V-band flux (right-hand and left-hand black points, Fig. 13). We know from Table 1 that the fraction of intrinsic BB disc flux in the V band is $f_d = 0.35$, i.e. $F_d(\nu_{\text{Vband}}) = f_d F_{\text{Vband}}$, which requires $r_{\text{out}} = 300$, in order to not overpredict the V-band disc flux.

Using the total band fluxes and the fractional contributions in Table 1, we can similarly constrain the UVW1 and V-band flux levels of the 6-d-lagged component (magenta squares, Fig. 13). We

then construct a BB spectrum that can supply these flux levels, shown in Fig. 13 by the magenta line. A BB spectral component has two parameters: its temperature and its area. The temperature defines the frequency of the BB peak, while the temperature and emitting area together determine the luminosity of the BB. We adjust the temperature until the peak is placed such that we can match the ratio of that component’s UVW1 to V-band flux. We then adjust the area of the BB reprocessor to give the BB the appropriate luminosity.

The grey crosses in Fig. 13 show the flux level of the component that varies as the observed FUV light curve (the flux level in the FUV band is found by subtracting the flux contributions of the other components from the total FUV flux). The spectral shape of this component is qualitatively similar to the Comptonized disc component shown in Fig. 7(a). Although the unlagged component dominates in the FUV band, there is some contamination from the lagged BB. We recalculate the FUV light curve including this contamination to check that it does not affect the CCF peak lags and find that its effect is negligible.

Separating the variability of the source into its different components and constraining the contribution of these components to different bands has allowed us to constrain the spectrum of the reprocessor. Assuming that this reprocessor is a BB emitter allowed us to constrain its temperature ($T = 9600$ K) and emitting area ($A = 3.04 \times 10^{30}$ cm², implying a luminosity $L_{\text{BB}} = 1.37 \times 10^{42}$ erg s⁻¹). The radial location of the reprocessor is constrained by its lag time, i.e. it must be located 6 light-days from the central source, which is $3240R_g$ for NGC 5548 with $M = 3.2 \times 10^7 M_\odot$. Hence, we can derive the covering factor, f_{cov} , of the reprocessor, since $f_{\text{cov}} = A/(2\pi R^2) = 0.002$. This is tiny and further underlines why the reprocessor cannot be a disc, which has a huge area at these radii.

A possible source of small-area reprocessors at large radii could be dense clumps originating in a dust-driven disc wind just like the broad-line-emitting clouds (Czerny et al. 2015), which are too dense to emit broad lines so instead reprocess the illuminating flux as thermal emission (see also Lawrence 2012). Knowing the covering fraction, it is clear that this material intercepts only 0.2 per cent of the illuminating flux. This is far too small to produce the observed luminosity required for the lagged component, given the observed

bolometric luminosity of the source ($\sim 2 \times 10^{44}$ erg s $^{-1}$; Mehdipour et al. 2015).

Hence, we can rule out the lag originating from the reprocessing of irradiating flux, where the reprocessing makes BB radiation and the lag is from the light travel time. Such a model fails on energetic grounds. A BB reprocessor at large radii ($\sim 2000\text{--}3000R_g$, as required by the lag times) must have a small area (ie. covering fraction), if it is to emit at a high enough temperature to contribute significant flux to UVW1 and the V band, which means it cannot intercept sufficient illuminating flux to reprocess and heat it to this required temperature.

It seems more likely that the lag is not simply from light travel time delays, but is instead lengthened by some response of the disc structure to the changing illuminating flux.

5.1 An alternative explanation for the UV/optical lags

So far, we have assumed that the FUV regions of the puffed-up, optically thick, Comptonized disc region illuminate some separate reprocessor – either a standard BB disc or optically thick BLR clouds. Having shown that neither reprocessor can produce the observed lags, we suggest that perhaps light travel time lags from an illuminating source to an external reprocessor are not involved at all; perhaps, the lags instead represent the lag time for the BB disc vertical structure to respond to changes in the FUV illumination.

In this scenario, the hard X-rays heat the inner (soft X-ray emitting) edge of the puffed-up Comptonized disc and this causes a heating wave, which dissipates outwards. From an examination of the observed light curves (Fig. 6), we know that this heating wave must quickly lose the high-frequency power of the hard X-rays, and it must also include some intrinsic fluctuations produced within the Comptonized disc itself. We speculate that an increase in the hard X-ray flux produces a stronger heating wave, which dissipates outwards through the Comptonized disc. When this heating wave reaches the outer edge of the Comptonized disc, this increases the FUV illumination of the surrounding BB disc. This illumination is concentrated on the innermost BB disc radii adjacent to the Comptonized disc. These BB disc radii respond to the increase in illumination by expanding upwards, becoming less dense and less able to thermalize, so they may switch from emitting BB radiation to emitting via optically thick Compton – the Comptonized disc region has essentially expanded outwards. When the hard X-ray flux decreases, there is less heating of the Comptonized disc region, and perhaps its outer radii can then cool and return to emitting BB. The Comptonized disc region is effectively breathing in and out in response to the X-ray heating of its inner edge. We suggest that this expanding and contracting of the puffed-up Comptonized disc region, i.e. this movement of the transition radius between Comptonized disc and BB disc, is then the cause of the inter-band UV–optical lags. The lag times should therefore reflect the response time of the disc vertical structure to changing irradiation.

The fastest response time-scale of the disc is the dynamical time-scale. This sets both the orbital time-scale and the time-scale on which the vertical structure responds to loss of hydrostatic equilibrium. The latter seems more appropriate for the physical mechanism we envisage, but this is 32 d for a mass of $3.2 \times 10^7 M_\odot$ at $200R_g$. It is only as short as 6 d for $70R_g$. Hameury et al. (2009) calculate the effect of the disc instability for an AGN, but their illumination geometry is for a central source rather than the larger scaleheight FUV illumination envisaged here. More detailed simulations are required to see if such a mechanism is feasible and, if so, how to determine the radius more precisely from the time-scale.

6 CONCLUSIONS

We have built a full disc reprocessing model in an attempt to simulate the simultaneous multiwavelength light curve data presented by Edelson et al. (2015), assuming that the UV/optical variability seen in NGC 5548 is due to reprocessing of higher energy radiation by a BB accretion disc. This higher energy radiation is traditionally assumed to be the hard X-ray power law, produced at small accretion flow radii. We find that reprocessing of the hard X-rays by a standard BB accretion disc cannot replicate the observed UV/optical light curves or their lags with respect to the illuminating X-rays. Specifically, the simulated light curves reproduce too much of the hard X-ray high-frequency power, and the light travel lag times are too short.

One obvious answer to increase the amount of smoothing and increase the light travel lag times would appear to be to make the BB accretion disc larger. The first reason this is not an option is a constraint from the spectral energy distribution of NGC 5548. We have limited the size of our model accretion disc to the self-gravity radius. We could relax this condition and allow the BB disc to extend to larger radii, but this would cause the disc spectrum to extend to lower energies. By contrast, the observed spectrum of NGC 5548, as shown by Mehdipour et al. (2015), clearly does not show such emission. The peak UV/optical emission occurs in the UVW1 bandpass and the emission below this energy rapidly drops off. With an outer disc radius at the self-gravity radius, we already slightly overpredict the lowest energy fluxes. However, we modelled this directly, and found that the radii required to smooth the reprocessed hard X-ray light curve to a level matching the data are so large that the resulting lag times are too long to be compatible with the observations.

We are then driven to a scenario where the reprocessor cannot directly see the hard X-rays. This requires some source of material with sufficient scaleheight such that it can block the optical-emitting regions' view of the hard X-rays. The obvious candidate for this is the extra component required to fit the soft X-ray excess.

There is much debate over the physical origin of this component. We envisage a scenario where it is produced in an optically thick Comptonizing region at larger radii than the central hard X-rays. UV/FUV emission produced in this region lifts material out of the plane of the accretion flow, where it is illuminated by the hard X-ray flux, which overionizes the material. The resultant loss of UV opacity means that it falls back down, resulting in a region with scaleheight sufficient to prevent the hard X-rays illuminating the outer BB disc. The soft X-ray emission could come from the inner radii of this Comptonized disc region, while the lowest energy FUV emission could come from its largest radii.

One problem with complete shielding is that the observed FUV and hard X-ray light curves *are* significantly correlated, though the correlation is quite poor. One possibility to incorporate some feedback between the two regions is if hard X-rays illuminate the inner edge of the Comptonized disc region, and these fluctuations then dissipate outwards through the Comptonized disc until they reach the outer FUV-emitting regions, which then illuminate the surrounding BB disc. It is then the dissipation of the hard X-ray fluctuations through the Comptonized disc component that causes the loss of high-frequency power, not light travel time smoothing. This dissipation process has to be extremely fast; however, the viscous time-scale in the Comptonized section of the disc should be faster than in a standard Shakura–Sunyaev BB disc.

We show that a model where the FUV emission (represented by the Hubble-band light curve) provides the illumination gives a much better match to the shape of the observed optical light

curves. However, our model response is still too fast at the longest wavelengths. The observed *V*-band lag in NGC 5548 is ~ 2 d behind the FUV emission, which requires the reprocessed *V*-band flux to be emitted at radii $R > 1000R_g$ for this source. However, BB disc annuli at these large radii are too cool to contribute significant flux to the *V* band, which is instead dominated by hotter emission from smaller BB disc radii with shorter lag times. The heating effect of the illuminating flux makes very little difference, as large disc annuli have an enormous area. The illuminating flux is simply spread over too large an area, so barely changes the temperature of the annulus and certainly cannot heat the annulus enough for it to contribute significant *V*-band flux. For the illuminating flux to heat a reprocessor at these large radii enough to contribute to the *V* band requires the reprocessor to have a small area.

We use the UV/optical light curves and CCFs to constrain the amount of reprocessed flux with different lag times in the UVW1 and *V* bands, and find that a combination of unlagged FUV light curve and FUV light curve lagged by 6 d can fit both bands. Assuming that this 6-d-lag reprocessed flux is BB emission, we then estimated the temperature and covering factor of the BB reprocessor and find $T = 9600$ K and $f_{\text{cov}} = 0.002$. This tiny covering factor rules out the BB disc as the source of the reprocessed emission. We consider the possibility that this emission may arise from optically thick BLR clouds that are too dense to emit via line emission so instead reprocess the FUV flux as thermal BB emission. However, this scenario is ruled out on energetic grounds – the inferred covering factor is too small for the reprocessor to intercept sufficient illuminating flux to heat it to the required temperature.

We conclude that the UV/optical light curves of NGC 5548 are not consistent with reprocessing of the hard X-rays by a BB accretion disc, but can instead be explained by reprocessing of the FUV emission where the lag is not a light travel time. We propose that the continuum lags of NGC 5548 are entirely generated by the ‘puffed-up’ Comptonized disc region of the accretion flow: The inner (soft X-ray emitting) edge of this region is heated by the hard X-rays, producing heating waves that dissipate outwards. The outer (UV/optical emitting) edge of the Comptonized disc then expands and contracts, in both radius and height, in response to the passage of these heating waves, and it is this behaviour that produces the continuum lags. The model still requires the presence of a standard outer Shakura–Sunyaev BB accretion disc, but this is a mostly constant component.

Ultimately, whatever the origin of the lags in NGC 5548, the data sets now available contain much more information than is encapsulated in a single lag time measurement. We urge full spectral–timing modelling of these data in order to extract all the new physical information on the structure and geometry of the accretion flow that is now within reach.

ACKNOWLEDGEMENTS

EG and CD acknowledge funding from the UK STFC grants ST/I001573/1 and ST/L00075X/1. CD acknowledges Missagh Mehdipour for multiple very helpful conversations and data, and Hagai Netzer for discussions about thermalization. We thank the referee for their detailed report that made us assess the energetics of our original reverse-engineered model with small clouds, and hence change the conclusions of our paper.

REFERENCES

Arévalo P., Uttley P., Lira P., Breedt E., McHardy I. M., Churazov E., 2009, *MNRAS*, 397, 2004

- Arévalo P., Uttley P., Kaspi S., Breedt E., Lira P., McHardy I. M., 2008, *MNRAS*, 389, 1479
- Bentz M. C. et al., 2010, *ApJ*, 716, 993
- Boissay R. et al., 2014, *A&A*, 567, A44
- Cackett E. M., Horne K., Winkler H., 2007, *MNRAS*, 380, 669
- Cackett E. M., Horne K., 2005, *Mem. Soc. Astron. Ital.*, 76, 47
- Capellupo D. M., Netzer H., Lira P., Trakhtenbrot B., Mejía-Restrepo J., 2015, *MNRAS*, 446, 3427
- Coleman M. S. B., Kotko I., Blaes O., Lasota J.-P., Hirose S., 2016, *MNRAS*, 462, 3710
- Crummy J., Fabian A. C., Gallo L., Ross R. R., 2006, *MNRAS*, 365, 1067
- Cunningham C., 1976, *ApJ*, 208, 534
- Czerny B. et al., 2015, *AdSpR*, 55, 1806
- Davis S. W., Woo J.-H., Blaes O. M., 2007, *ApJ*, 668, 682
- Denney K. D. et al., 2010, *ApJ*, 721, 715
- Done C., Davis S. W., Jin C., Blaes O., Ward M., 2012, *MNRAS*, 420, 1848
- Edelson R. et al., 2015, *ApJ*, 806, 129
- Fausnaugh M. M. et al., 2016, *ApJ*, 821, 56
- Gaskell C. M., Peterson B. M., 1987, *ApJS*, 65, 1
- Gierliński M., Done C., 2004, *MNRAS*, 349, L7
- Haardt F., Maraschi L., 1991, *ApJ*, 380, L51
- Haardt F., Maraschi L., 1993, *ApJ*, 413, 507
- Hameury J.-M., Viallet M., Lasota J.-P., 2009, *A&A*, 496, 413
- Heil L. M., Uttley P., Klein-Wolt M., 2015, *MNRAS*, 448, 3348
- Ingram A., Done C., 2012, *MNRAS*, 419, 2369
- Ingram A., Done C., Fragile P. C., 2009, *MNRAS*, 397, L101
- Jiang Y.-F., Davis S. W., Stone J. M., 2016, *ApJ*, 827, 10
- Jin C., Ward M., Done C., 2012, *MNRAS*, 425, 907
- Korista K. T., Goad M. R., 2001, *ApJ*, 553, 695
- Kotov O., Churazov E., Gilfanov M., 2001, *MNRAS*, 327, 799
- Laor A., Netzer H., 1989, *MNRAS*, 238, 897
- Laor A., Davis S. W., 2014, *MNRAS*, 438, 3024
- Lasota J.-P., 2001, *New Astron. Rev.*, 45, 449
- Lawrence A., 2012, *MNRAS*, 423, 451
- McHardy I. M. et al., 2014, *MNRAS*, 444, 1469
- McHardy I. et al., 2016, *ApJ*, 337, 500
- Malzac J., Dumont A. M., Mouchet M., 2005, *A&A*, 430, 761
- Matt G. et al., 2014, *MNRAS*, 439, 3016
- Mehdipour M. et al., 2015, *A&A*, 575, A22
- Morgan C. W., Kochanek C. S., Morgan N. D., Falco E. E., 2010, *ApJ*, 712, 1129
- Narayan R., Yi I., 1995, *ApJ*, 452, 710
- Noda H., 2016, *X-ray Studies of the Central Engine in Active Galactic Nuclei with Suzaku*, Springer theses. Springer Science+Business Media Singapore
- Noda H., Makishima K., Uehara Y., Yamada S., Nakazawa K., 2011, *PASJ*, 63, 449
- Pancoast A., Brewer B. J., Treu T., Park D., Barth A. J., Bentz M. C., Woo J.-H., 2014, *MNRAS*, 445, 3073
- Pancoast A., Brewer B. J., Treu T., Park D., Barth A. J., Bentz M. C., Woo J.-H., 2015, *MNRAS*, 448, 3070
- Peterson B. M. et al., 2002, *ApJ*, 581, 197
- Petrucci P. O., Ferreira J., Henri G., Malzac J., Foellmi C., 2010, *A&A*, 522, A38
- Petrucci P.-O. et al., 2013, *A&A*, 549, A73
- Porquet D., Reeves J. N., O’Brien P., Brinkmann W., 2004, *A&A*, 422, 85
- Sergeev S. G., Doroshenko V. T., Golubinskiy Y. V., Merkulova N. I., Sergeeva E. A., 2005, *ApJ*, 622, 129
- Stern B. E., Poutanen J., Svensson R., Sikora M., Begelman M. C., 1995, *ApJ*, 449, L13
- Svensson R., Zdziarski A. A., 1994, *ApJ*, 436, 599
- Ursini F. et al., 2015, *A&A*, 577, A38
- Uttley P., Edelson R., McHardy I. M., Peterson B. M., Markowitz A., 2003, *ApJ*, 584, L53
- Welsh W. F., Horne K., 1991, *ApJ*, 379, 586
- Zycki P. T., Done C., Smith D. A., 1999, *MNRAS*, 305, 231

This paper has been typeset from a $\text{\TeX}/\text{\LaTeX}$ file prepared by the author.